ANL-7927
Reactor Technology

ARGONNE NATIONAL LABORATORY
9700 South Cass Avenue
Argonne, Illinois 60439

ACTIVATION-RATE MEASUREMENTS IN THE ZPR-3 MOCKUP CRITICAL EXPERIMENTS

Part III. Measurements of Foil-activation Rates in Assemblies 62 and 63 of ZPR-3 Mockups of EBR-II with a Stainless Steel Reflector

by

N. D. Dudey, R. J. Popek, and R. R. Heinrich

Chemical Engineering Division

June 1972

Previous reports in this series

Part I: ANL-7781

Part II: ANL-7926

DISCLAIMER

TABLE OF CONTENTS

LIST OF FIGURES

LIST OF TABLES

LIST OF TABLES (Continued)

ACTIVATION-RATE MEASUREMENTS IN THE ZPR-3 MOCKUP CRITICAL EXPERIMENTS

Part III. Measurements of Foil-activation Rates in Assemblies 62 and 63 of ZPR-3 Mockups of EBR-II with a Stainless Steel Reflector

by

N. D. Dudey, R. J. Popek, and R. R. Heinrich

ABSTRACT

This is the third and last report in a series describing activation-rate measurements conducted in the ZPR-3 critical facility, which was mocked up to simulate various configurations of EBR-II. The primary objective of the series is to describe the measurements in sufficient detail to allow the results to be evaluated by the reader and used as deemed appropriate. The present report gives a complete description of the activation-rate measurements conducted in Assemblies 62 and 63 of ZPR-3. Both assemblies simulated EBR-II with a stainless steel reflector. They differed in that Assembly 62 represented a homogeneous core with a composition similar to EBR-II, whereas Assembly 63 was composed of a heterogeneous series of drawer loadings and represented a more "typical" EBR-II core loading.

In Assembly 62, foil-activation-rate measurements were made in three principal locations, near the core center, near the core-blanket interface, and within the radial reflector. In Assembly 63, foil-activation-rate measurements of only ^{235}U and ^{238}U were made at 15 different drawer locations. The Assembly 63 experiment provided fission-rate traverses, as well as an examination of the effects that various types of drawer loadings had upon the fission rates. For Assembly 62, the reaction-rate data are presented, intercompared, and also compared with the results from another activation-rate experiment performed by the Applied Physics Division. Assembly 63 fission rates determined by foil activation are compared with results obtained by fission-counter traverses.

I. INTRODUCTION

This report, which is the third in a series of reports describing the results of foil-activation-rate measurements conducted in the ZPR-3 mockup program, specifically discusses the activation-rate measurements conducted in Assemblies 62 and 63 of ZPR-3. Assembly 62 measurements were very similar to the Assembly 60 and 61 measurements previously reported.[1,2] These two earlier reports must be considered an integral part of the present report, and together, the three reports constitute a complete presentation of the activation-rate measurements in the EBR-II mockup critical program.

Assembly 62 differed from the other assemblies in that the first four drawers of the reflector region consisted of stainless steel, whereas the reflector region was ^{238}U in Assembly 60, and nickel in Assembly 61. Assembly 63 contained the same axial and radial reflectors as those used in Assembly 62 but differed in the core configuration. The core of Assembly 63 was designed to simulate a "typical" EBR-II core configuration, that is, it was composed of heterogeneous elements simulating full and partial ^{235}U-fueled drivers, full and partial plutonium-uranium oxide drivers, ^{235}U-fueled control and safety subassemblies, and structural-type subassemblies.

The objectives of the overall EBR-II mockup critical program were discussed in the first report[1] in this series. The specific objective of Assembly 62 was to provide reaction-rate results obtained with a stainless steel-reflected configuration that could be compared directly with results obtained with uranium- and nickel-reflected configurations. To achieve this comparison, the four rows of the radial reflector region adjacent to the core were suitably altered in Assemblies 60, 61, and 62, and only very minor changes were made in the core compositions to achieve the optimum critical configuration. The specific objective of Assembly 63 was to alter the core composition to simulate a heterogeneous subassembly composition typical of EBR-II, while preserving the reflector-blanket configuration of Assembly 62. With this alteration, fission-rate measurements could be made that would directly reflect the heterogeneous effects of the subassembly simulations.

II. EXPERIMENTAL

A. Assembly 62

1. Description of Irradiation

The composition of the core of Assembly 62 was identical to that of the core of Assembly 61.[2] The only significant change in Assembly 62, as compared with Assembly 61, was the replacement of the nickel radial reflector used in Assembly 61 with a stainless steel-rich reflector. The Assembly 62 critical configuration contained 221.61 kg of ^{235}U and had an excess reactivity of 0.146% $\Delta K/K$.[3] A vertical cross-section view of the reference loading is shown in Fig. 1. The average compositions of the core, stainless steel radial-reflector, and uranium radial-blanket regions are given in Table I. A more complete description of Assembly 62 is given in Ref. 3.

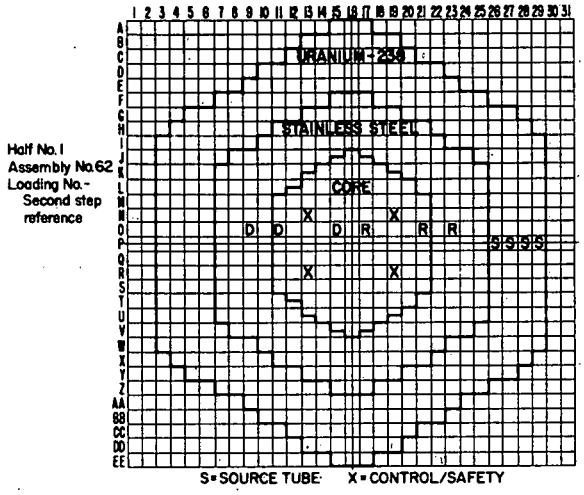

Fig. 1

Matrix Pattern and Foil-packet Locations in Assembly 62 (Vertical Cross Section of Half No. 1)

TABLE I. Average Compositions of Assembly 62 Zones (10^{24} atoms/cc)

Element	Core Average	SS Reflector	Uranium Blanket
U-235	0.005080		0.000055
U-238	0.005053		0.026502
Na	0.01033	0.00205	0.00456
Fe	0.01337	0.04900	0.00964
Cr	0.00343	0.01348	0.00254
Ni	0.00149	0.00578	0.00110
Mn	0.000172	0.000977	0.000145
Si	0.00013	0.000388	0.00007
Mo	-	0.000072	-
O	0.002135		-

The foil packets irradiated in Assembly 62 were of two types. The dosimetry-type packets located in the three D positions (see Fig. 1) were identical. These packets contained 1.97-in. square metal foils of aluminum, nickel, gold, ^{235}U, and ^{238}U. The nominal thickness was 10 mils for the aluminum, nickel, and ^{238}U foils, 0.2 mil for each of the three gold foils in a packet, and 6 mils for the ^{235}U foils. The uranium foils were individually wrapped in commercial-grade aluminum foil (0.5 mil) to contain any recoil fission fragments and to minimize cross contamination between foils. Enrichments for ^{235}U and ^{238}U were 93.1% and 99.8%, respectively. All the individual foils were wrapped together in aluminum foil to constitute a packet. Each packet weighed about 28 grams, and was

inserted into the assembly drawer perpendicularly to the drawer plates and about 1 in. from the front of the drawer. All drawers were located just above the physical midplane of the core in Half 1.

The other type of foil packet, designated R in Fig. 1, consisted of one 0.2-mil-thick gold foil and one 10-mil-thick nickel foil. Uranium and aluminum were not included in these packets. The R packets were packaged identically to the D packets and were located in positions symmetric with the D foils. The R positions were identical to those in which the fission-yield foils had been placed in Assemblies 60 and 61. The objective of the positioning was to determine whether flux symmetry existed for the physically symmetric locations. Since the $^{58}Ni(n,p)$ reaction is sensitive only to neutrons above $\sim$1 MeV and the $^{197}Au(u,\gamma)$ reaction is primarily sensitive to neutrons below 1 MeV, the nickel and gold foils would also permit examination of spectral symmetry within the Assembly.

The six R and D foil packets were irradiated in Assembly 62 for 60 minutes at a reactor power level comparable to those of the Assembly 60 and 61 irradiations. The irradiation was terminated at 1109 MDT on Sept. 24, 1970. The foil packets were received at Argonne-Illinois for analysis about 24 hr after the end of the irradiation.

2. Analysis of the Irradiated Samples

The irradiated foil packets were opened and the 2-in. by 2-in. foils were cut into smaller pieces for counting. The cutting pattern was designed to maximize the effects of heterogeneity upon the foils that resulted from the plate composition of the assembly drawers and to allow correlation of these effects with the activation-rate measurements from the Assembly 60 and 61 experiments. Figure 2 shows the cutting pattern and the orientation of the cut pieces relative to the plate configuration of the drawers.

After cutting, the individual pieces were weighed and mounted on aluminum discs for gamma-counting. The fissionable foils were cut with the aluminum recoil catcher intact; the aluminum was removed for weighing of the uranium, but both were mounted together for counting. The weights of the D samples are given in Tables II and III and the weights of the R samples are given in Table IV.

The gamma-counting and data analysis for all Assembly 62 samples were identical to the two previous Assemblies (60 and 61), and are described in detail in Ref. 1 and 2. Reference 2 also describes the improvements in detector efficiencies and fission yields that were applied to the Assembly 61 results. These improvements were also applied to the Assembly 62 and 63 results described here.

B. Assembly 63

1. Description of Irradiation

The Assembly 63 core loading was designed to simulate a typical loading of EBR-II. Various types of EBR-II subassemblies were simulated by adjusting the composition of a single ZPR-3 matrix drawer to approximate closely the atom ratios present in an EBR-II subassembly. The loading

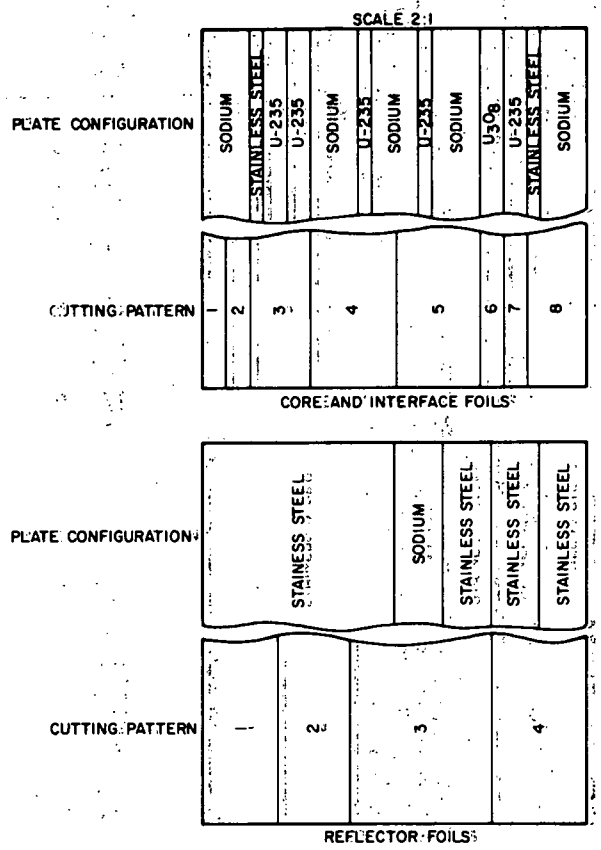

Fig. 2. Plate Configuration, Composition, and Sample Cutting Pattern for Core and Reflector Drawers of Assembly 62

TABLE II. Weights of ^{235}U, ^{238}U, Al, and Ni Dosimetry Samples Irradiated in Assembly 62

^{235}U		^{238}U		Al		Nickel	
Sample No.	Wt (mg)	Sample No.	Wt (mg)	Sample No.	Wt (mg)	Sample No.	Wt (mg)
5R 1	1467.1	8R 1	2326.0	AR 1	335.5	NR 1	1091.0
2	1391.5	2	2313.7	2	325.3	2	1070.3
3	2756.9	3	4588.0	3	642.0	3	2132.2
4	1653.6	4	2736.5	4	421.7	4	1363.0
5I 1	417.3	8I 1	663.7	AI 1	108.0	NI 1	339.2
2	429.0	2	706.3	2	110.7	2	363.2
3	1139.1	3	1843.8	3	281.6	3	925.6
4	1524.2	4	2462.8	4	376.0	4	1235.3
5	1556.3	5	2448.6	5	380.1	5	1253.2
6	436.5	6	677.3	6	109.2	6	353.8
7	428.8	7	693.4	7	110.1	7	359.6
8	953.1	8	1389.6	8	249.9	8	822.4
5C 1	315.2	8C 1	636.2	AC 1	107.0	NC 1	329.3
2	429.7	2	721.4	2	111.9	2	357.4
3	1130.1	3	1891.9	3	279.4	3	923.6
4	1581.2	4	2579.8	4	375.4	4	1228.9
5	1631.5	5	2644.7	5	380.6	5	1247.2
6	454.8	6	757.2	6	108.0	6	355.0
7	453.7	7	768.4	7	110.0	7	356.2
8	984.0	8	1716.8	8	249.6	8	826.0

TABLE III. Weights of Gold Dosimetry Samples Irradiated in Assembly 62

Front Foil		Middle Foil		Back Foil	
Sample No.	Wt (mg)	Sample No.	Wt (mg)	Sample No.	Wt (mg)
1GR 1	43.6	2GR 1	44.6	3GR 1	43.8
2	41.9	2	41.7	2	42.3
3	84.5	3	85.1	3	83.9
4	54.5	4	53.5	4	53.6
1GI 1	13.5	2GI 1	14.6	3GI 1	14.9
2	13.4	2	15.2	2	14.3
3	36.1	3	39.8	3	38.6
4	48.6	4	52.5	4	50.1
5	50.6	5	53.5	5	49.8
6	14.1	6	14.2	6	13.8
7	15.1	7	15.5	7	14.5
8	33.9	8	35.1	8	31.1
GC 1	15.0				
2	14.6				
3	38.8				
4	51.7				
5	52.8				
6	14.7				
7	15.1				
8	35.4				

TABLE IV. Weights of Gold and Nickel R-packet Samples Irradiated in Assembly 62

Gold		Nickel	
Sample No.	Wt (mg)	Sample No.	Wt (mg)
RGR 1	42.7	RNR 1	1099.3
2	40.6	2	1061.8
3	82.7	3	2121.8
4	54.2	4	1350.0
RGI 1	14.2	RNI 1	337.2
2	14.2	2	363.1
3	36.8	3	927.3
4	48.9	4	1241.9
5	49.8	5	1245.4
6	14.1	6	356.4
7	14.3	7	355.2
8	31.5	8	825.5
RGC 1	14.2	RNC 1	313.1
2	13.5	2	361.4
3	37.9	3	935.9
4	49.9	4	1237.6
5	50.4	5	1257.0
6	13.8	6	352.8
7	14.6	7	360.8
8	31.7	8	845.5

consisted of six simulated structural elements, nine simulated 19-pin oxide elements, nine simulated 37-pin oxide elements, 14 simulated EBR-II control/safety elements, and 17 partial ^{235}U-fueled driver elements. The remaining core locations contained drawers simulating full ^{235}U-fueled driver elements. A vertical cross-section view of the reference loading is shown in Fig. 3. The average compositions of the individual elements are presented in Table V. The critical configuration contained 196.58 kg of ^{235}U and a total of 7.75 kg of ^{239}Pu and ^{241}Pu, and had an excess reactivity of 0.71×10^{-3} $\Delta K/K$.[4] The radial reflector and blanket regions were the same as those constructed in Assembly 62; their average compositions are given in Table I. A more detailed description of Assembly 63 is given in Ref. 4.

The foil-activation measurements in Assembly 63 consisted of ^{235}U and ^{238}U fission-rate measurements at 15 selected locations. The foil packets consisted of 1.97-in. square metal foils of ^{238}U and ^{235}U indivdually wrapped in 0.5-mil aluminum. The nominal foil thicknesses varied from 2 to 3 mils for ^{235}U and from 6 to 10 mils for ^{238}U. The two foils were wrapped together in aluminum to form a packet. These packets were inserted

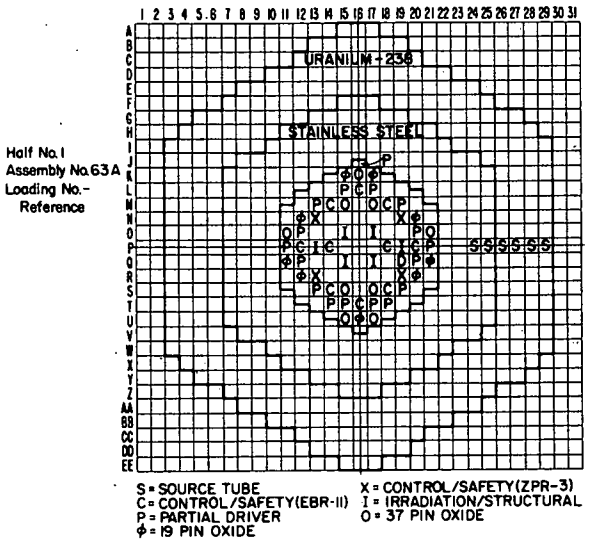

Fig. 3

Matrix Pattern of Assembly 63 (Vertical Cross Section of Half No. 1)

into the assembly drawers perpendicularly to the plates in the drawers and were located two inches from the front of the drawers in Half 1. The 15 locations at which the packets were irradiated are shown in Fig. 4. All foil packets were irradiated simultaneously for 60 minutes at a reactor power level comparable to those of the previous irradiations. The irradiation was terminated at 1111 CST on Nov. 11, 1970.

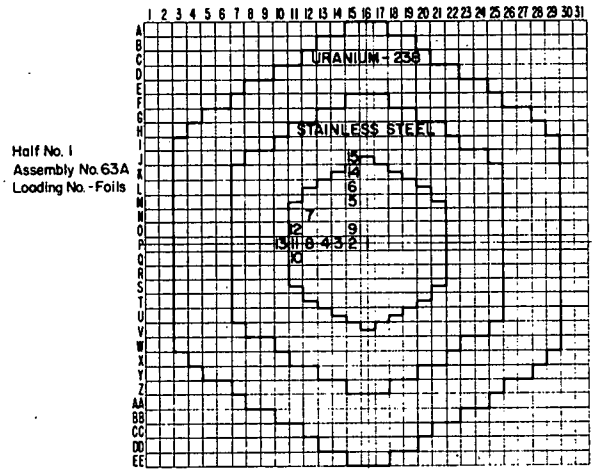

Fig. 4

Foil-packet Locations in Assembly 63

2. Analysis of the Irradiated Samples

After irradiation, the 2-in. square foils were cut into four 1-in. square pieces for gamma-counting. This cutting pattern was chosen to provide better spatial sensitivity than the whole 2-in.-square could provide, but yet yield pieces large enough so that the heterogeneity effects caused by the plate geometry could be minimized. The cutting pattern and

TABLE V. Core-averaged Compositions for Assembly 63
(Units: 10^{24} atoms/cc)

Element	Partial Driver	Full Driver	37-pin Oxide	19-pin Oxide	Control and Safety--EBR-II	Control and Safety--ZPR-3	Structural
^{235}U	0.003404	0.006912	0.004472	0.002236	0.004722	0.004717	-
^{238}U	0.003858	0.006248	0.0003189	0.0001594	0.004898	0.002495	-
^{239}Pu and ^{241}Pu	-	-	0.001067	0.001067	-	-	-
^{240}Pu and ^{242}Pu	-	-	0.0000508	0.0000508	-	-	-
Na	0.01043	0.01043	0.008343	0.006602	0.01251	0.01251	0.004176
O	-	-	0.01334	0.008003	-	-	-
Fe	0.01988	0.01218	0.01968	0.02973	0.01152	0.01573	0.04579
Cr	0.004946	0.003029	0.002599	0.006018	0.002867	0.003912	0.01139
Ni	0.002164	0.001326	0.001137	0.002633	0.001255	0.001712	0.004984
Mn	0.0002064	0.0001265	0.0001085	0.0002513	0.0001197	0.0001633	0.0004756
Si	0.0002397	0.0001485	0.0001273	0.0002950	0.0001403	0.0001916	0.0005582

sample numbering scheme are shown in Fig. 5. The first digit of the numbering scheme refers to the packet number, the second defines the isotope, and the third identifies the location within the 2-in. square.

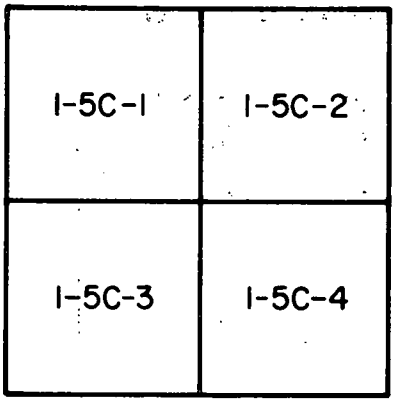

Fig. 5

Cutting Pattern and Sample-identification Scheme for Foil Packets in Assembly 63

After cutting, the individual pieces were weighed and mounted on 1/16-in.-thick aluminum discs for gamma-counting. The weights of the samples, together with their identification number and matrix position at which they were irradiated, are presented in Tables VI and VII.

Gamma-assay of the samples and analysis of the data were identical to those used in the three previous Assembly experiments (see Ref. 1 for details), with the exception that all samples from Assembly 63 were counted on an automatic sample-changer system. This system consisted of a Ge(Li) detector with a 2.2 keV resolution, a 4096-channel analyzer, and a magnetic-tape readout. All considerations related to corrections to the data and analysis of errors are described in Ref. 1 and are pertinent to the present data.

III. RESULTS

The absolute reaction rates have been computed from the following equation:

$$(\bar{\sigma}\phi) = \frac{\lambda N_o}{n(1-e^{-\lambda t})} \qquad (1)$$

where N_o is the measured number of reaction-product atoms present at the end of the irradiation, λ is the decay constant for the reaction product expressed in units of sec^{-1}, n is the number of target atoms irradiated in the sample, t is the time of the irradiation. The reaction rates, $\bar{\sigma}\phi$, are thus expressed in units of atoms of reaction product per target atom-second, or more simply, sec^{-1}. A thorough discussion of the error analysis was presented in Ref. 1 and the equations used for propagation of errors are described by Equations 2-4 of that reference.

TABLE VI. Weights of ^{235}U Dosimetry Samples Irradiated in Assembly 63

Matrix Location	Sample No.	Wt (g)	Matrix Location	Sample No.	Wt (g)	Matrix Location	Sample No.	Wt (g)
P-16	1-5C-1	0.6204	L-15	6-5C-1	0.6369	P-11	11-5C-1	0.9744
	2	0.6155		2	0.6235		2	0.9681
	3	0.6176		3	0.6253		3	0.9530
	4	0.6216		4	0.6216		4	0.9656
P-15	2-5C-1	0.6254	N-12	7-5C-1	0.6313	O-11	12-5C-1	0.9671
	2	0.6179		2	0.6203		2	0.9522
	3	0.6156		3	0.6228		3	0.9529
	4	0.6141		4	0.6200		4	0.9551
P-14	3-5C-1	0.6289	P-12	8-5C-1	0.6361	P-10	13-5C-1	0.9674
	2	0.6211		2	0.6254		2	0.9638
	3	0.6160		3	0.6295		3	0.9516
	4	0.6213		4	0.6276		4	0.9615
P-13	4-5C-1	0.6330	O-15	9-5C-1	0.6389	K-15	14-5C-1	0.9555
	2	0.6179		2	0.6260		2	0.9449
	3	0.6294		3	0.6295		3	0.9559
	4	0.6207		4	0.6237		4	0.9758
M-15	5-5C-1	0.6323	Q-11	10-5C-1	0.9683	J-15	15-5C-1	0.9672
	2	0.6208		2	0.9591		2	0.9513
	3	0.6241		3	0.9568		3	0.9586
	4	0.6196		4	0.9596		4	0.9684

TABLE VII. Weights of ^{238}U Dosimetry Samples Irradiated in Assembly 63

Matrix Location	Sample No.	Wt (g)	Matrix Location	Sample No.	Wt (g)	Matrix Location	Sample No.	Wt (g)
P-16	1-8C-1	1.6530	L-15	6-8C-1	2.8842	P-11	11-8C-1	2.5550
	2	1.6262		2	2.8422		2	2.7371
	3	1.6449		3	2.8799		3	2.8909
	4	1.6846		4	2.9166		4	3.1586
P-15	2-8C-1	1.6168	N-12	7-8C-1	3.0307	O-11	12-8C-1	2.6992
	2	1.5901		2	2.8956		2	2.9021
	3	1.6324		3	3.0541		3	2.8143
	4	1.6770		4	3.0206		4	3.0966
P-14	3-8C-1	1.6340	P-12	8-8C-1	2.8132	P-10	13-8C-1	2.7399
	2	1.5970		2	2.7467		2	2.8891
	3	1.6247		3	2.8048		3	2.8823
	4	1.6551		4	2.8554		4	3.0832
P-13	4-8C-1	1.5639	O-15	9-8C-1	2.8477	K-15	14-8C-1	2.7876
	2	1.5425		2	2.6942		2	2.9486
	3	1.5771		3	2.8070		3	2.9026
	4	1.6162		4	2.7309		4	3.1264
M-15	5-8C-1	1.6060	Q-11	10-8C-1	2.6603	J-15	15-8C-1	2.8496
	2	1.5961		2	2.8680		2	2.7725
	3	1.6150		3	2.7628		3	2.9610
	4	1.6429		4	3.0401		4	2.8149

A. Assembly 62

Table VIII presents the absolute reaction rates for the reactions $^{58}Ni(n,p)^{58}Co$, $^{27}Al(n,\alpha)^{24}Na$, and $^{238}U(n,\gamma)^{239}Np$ measured from the dosimetry-foil packets irradiated at the core, core-reflector interface, and reflector locations in Assembly 62. The matrix positions within the assembly to which these locations correspond are also indicated in Table VIII. The errors in the absolute reaction rates for these three reactions are 5.9%, 8.0%, and 6.0-6.8%, respectively.

Table IX summarizes the absolute reaction rates for the $^{197}Au(n,\gamma)^{198}Au$ reactions measured from the dosimetry-foil packets. The absolute error of this reaction rate is 8.1% for all measurements. The front, middle, and back foils refer to the three gold foils irradiated in the interface and reflector positions for the purpose of evaluating neutron self-absorption effects within the gold foils.

Table X summarizes the absolute reaction rates for the $^{197}Au(n,\gamma)^{198}Au$ and $^{58}Ni(n,p)^{58}Co$ reactions measured from the foils irradiated on the right side of the assembly. The absolute errors of these reactions are 8.1% and 5.8%, respectively.

Tables XI and XII summarize the absolute production rates of the individual fission products measured in the ^{235}U and ^{238}U foils, respectively. The absolute fission rate of a sample was determined by dividing the sum of the individual fission-product rates by the sum of the fission yields for each nuclide. The fission yields used for this determination are given in Table X of reference 2. The results of the fission-rate measurements for ^{235}U and ^{238}U are presented in Table XIII. The relative errors were evaluated by propagating the uncertainty in each individual fission-product activity to obtain the overall uncertainty for the sum. The absolute fission-rate error is dominated by uncertainties in the fission yields, which are estimated to be accurate to ±10%.

For the purpose of neutron spectral analysis of the reactor, it is convenient to examine ratios of selected reaction rates. Table XIV summarizes the spectrum-averaged cross-section ratios measured in Assembly 62.

The results presented above enable us to examine the detailed heterogeneity effects within the drawers of Assembly 62. A more general comparison of data can be made by averaging the individual reaction rates of the samples at a given drawer location; this averaging yields drawer-averaged reaction rates. The drawer-averaged reaction rates were determined by averaging on the basis of the weight of each sample.

In addition to the measurements reported here, other activation-rate measurements were performed in Assembly 62 by Maddison;[5] in these experiments disc foils were irradiated between the fuel plates at locations symmetric with those used in our measurements. These results are reported in units of gram-hr^{-1}, and must be converted to our units before comparison can be made with our drawer-averaged reaction rates. In addition, Maddison's fission-rate values were determined by measuring only the ^{97}Zr fission product and applying a fission-yield value of 5.77% for ^{235}U and a value of 5.99% for ^{238}U. To provide a consistent basis for comparison,

TABLE VIII. Absolute Reaction Rates for $^{58}Ni(n,p)^{58}Co$, $^{27}Al(n,\alpha)^{24}Na$ and $^{238}U(n,\gamma)^{239}Np$ in Assembly 62

Sample		Absolute Reaction Rate [10^{-16} atoms/atom-sec]					
		$^{58}Ni(n,p)^{58}Co$		$^{27}Al(n,\alpha)^{24}Na$		$^{238}U(n,\gamma)^{239}Np$	
		Rate	Relative Error (%)	Rate	Relative Error (%)	Rate	Relative Error (%)
Reflector (0-9)	1	0.413	0.8	0.00177	3.3	48.6	1.2
	2	0.485	0.3	0.00201	3.0	49.1	1.0
	3	0.591	0.6	0.00244	0.7	49.1	0.9
	4	0.736	0.3	0.00312	2.0	48.2	1.1
Interface (0-11)	1	2.90	0.3	0.0142	4.4	32.8	1.3
	2	3.04	0.5	0.0151	0.1	31.7	1.1
	3	3.36	0.3	0.0177	0.1	28.9	1.0
	4	3.59	0.4	0.0185	1.6	27.7	1.3
	5	3.94	0.1	0.0206	0.2	27.4	1.1
	6	4.30	0.3	0.0231	2.2	26.6	1.4
	7	4.41	0.1	0.0229	1.3	27.1	1.4
	8	4.32	0.2	0.0221	1.4	28.1	1.3
Core (0-15)	1	6.71	0.3	0.0335	0.2	36.1	0.8
	2	6.72	0.1	0.0347	1.0	35.4	0.9
	3	6.89	0.1	0.0356	2.2	34.9	1.1
	4	6.64	0.1	0.0355	0.4	35.3	1.3
	5	6.79	0.1	0.0353	0.6	35.6	1.5
	6	7.13	0.2	0.0368	0.4	36.1	0.9
	7	7.15	0.6	0.0370	1.3	35.8	0.9
	8	6.89	0.1	0.0353	1.1	35.2	0.9

TABLE IX. $^{197}Au(n,\gamma)^{198}Au$ Absolute Reaction Rates for Dosimetry Samples in Assembly 62

		Absolute Reaction Rate [10^{-16} atoms/atom-sec]					
		Front Foil		Middle Foil		Back Foil	
		Rate	Relative Error (%)	Rate	Relative Error (%)	Rate	Relative Error (%)
Reflector (0-9)	1	220	0.2	202	0.5	226	0.1
	2	216	0.1	202	0.2	223	0.5
	3	208	0.5	195	0.2	218	0.9
	4	199	0.5	185	0.1	207	0.2
Interface (0-11)	1	87.7	0.1	85.8	0.2	88.6	0.6
	2	83.4	0.1	81.6	0.2	85.8	0.5
	3	70.8	0.4	68.7	0.2	71.2	0.1
	4	62.3	0.1	61.0	0.1	62.8	0.1
	5	57.5	0.2	57.0	0.4	58.3	0.1
	6	54.7	0.5	53.7	0.1	56.2	0.6
	7	53.4	0.3	52.4	0.7	54.5	0.9
	8	52.8	0.2	52.3	0.5	53.4	0.2
Core (0-15)	1	57.2	0.5				
	2	56.5	0.1				
	3	56.0	0.3				
	4	58.2	0.4				
	5	58.4	0.3				
	6	57.4	0.4				
	7	56.6	0.1				
	8	57.7	0.5				

TABLE X. Absolute Reaction Rates of $^{197}Au(n,\gamma)^{198}Au$ and $^{58}Ni(n,p)^{58}Co$ for R Samples in Assembly 62

Sample Position		Absolute Reaction Rate [10^{-16} atoms/atom-sec] $^{197}Au(n,\gamma)^{198}Au$ Rate	Relative Error (%)	$^{58}Ni(n,p)^{58}Co$ Rate	Relative Error (%)
Reflector (0-23)	1	279	0.2	0.673	0.1
	2	298	0.1	0.560	0.1
	3	313	0.9	0.430	0.1
	4	315	0.5	0.335	0.4
Interface (0-21)	1	55.5	0.5	4.36	0.7
	2	55.7	0.1	4.32	0.1
	3	57.3	0.3	4.28	0.1
	4	63.7	0.1	3.79	0.3
	5	69.8	1.3	3.59	0.3
	6	72.9	0.3	3.59	0.7
	7	83.2	0.2	3.48	0.5
	8	100	0.1	3.01	0.5
Core (0-17)	1	57.7	0.1	6.86	0.4
	2	57.6	0.3	6.90	0.3
	3	57.2	0.1	7.01	0.4
	4	59.0	0.2	6.73	0.6
	5	58.4	0.7	6.72	0.9
	6	56.3	1.4	6.98	0.1
	7	56.7	0.7	7.07	0.2
	8	56.4	0.3	6.63	0.1

TABLE XI

^{235}U Absolute Fission-product Rates in Assembly 62

[10^{-15} atoms/(atom ^{235}U)(sec)]

Sample	^{95}Zr		^{97}Zr		^{103}Ru		^{131}I		^{132}Te		^{133}I		^{140}Ba		^{143}Ce	
	Rate	Abs Error, %	Rate	Abs Error, %	Rate	Abs Error, %	Rate	Abs Error, %	Rate	Abs Error, %	Rate	Abs Error, %	Rate	Abs Error, %	Rate	Abs Error, %
Reflector 1	1.68	3.8	1.56	3.8	0.815	5.6	0.800	3.3	1.12	5.8	1.69	5.0	1.45	3.4	1.20	2.6
2	1.72	3.8	1.60	2.8	0.849	3.3	0.834	3.8	1.13	6.4	1.78	3.1	1.48	2.7	1.16	3.4
3	1.74	3.4	1.54	4.0	0.824	2.8	0.821	5.5	1.25	7.0	1.85	6.6	1.50	2.7	1.20	2.7
4	1.80	4.0	1.62	3.2	0.853	3.0	0.850	3.4	1.25	6.2	1.91	4.6	1.49	4.4	1.17	4.1
Interface 1	1.64	3.7	1.52	3.5	0.799	2.9	0.781	3.0	1.19	5.6	1.59	3.2	1.48	3.0	1.28	3.2
2	1.50	4.6	1.32	5.6	0.794	3.6	0.798	2.5	1.16	6.0	1.58	3.3	1.41	2.6	1.29	2.6
3	1.50	4.9	1.39	3.8	0.791	3.6	0.776	3.0	1.17	6.4	1.67	4.5	1.38	3.4	1.25	2.8
4	1.48	4.7	1.41	4.3	0.768	4.1	0.782	3.3	1.17	5.9	1.65	2.6	1.43	4.2	1.29	3.3
5	1.52	4.6	1.44	5.4	0.790	4.5	0.794	2.8	1.18	6.7	1.62	2.8	1.37	3.2	1.28	3.3
6	1.57	4.4	1.47	5.0	0.833	3.6	0.816	2.8	1.20	5.7	1.65	2.9	1.41	2.6	1.22	3.4
7	1.60	4.9	1.47	5.4	0.832	3.9	0.857	2.7	1.17	6.1	1.63	4.6	1.47	2.6	1.30	4.0
8	1.55	4.6	1.49	4.1	0.815	3.5	0.798	2.8	1.15	5.7	1.66	2.5	1.39	3.0	1.30	4.4
Core 1	2.15	4.8	2.07	5.1	1.17	4.6	1.15	2.7	1.58	5.8	2.23	3.6	2.00	2.5	1.75	4.3
2	2.12	4.6	2.00	3.6	1.13	3.5	1.12	2.7	1.60	6.4	2.13	2.6	1.95	2.6	1.82	3.5
3	2.17	5.5	2.02	4.4	1.10	3.5	1.15	2.5	1.63	5.5	2.12	3.3	1.92	2.8	1.84	3.8
4	2.12	4.4	2.06	5.1	1.09	3.6	1.10	2.9	1.62	6.4	2.20	2.9	1.90	2.6	1.68	2.8
5	2.15	4.3	1.99	4.4	1.10	3.8	1.10	3.2	1.67	6.4	2.27	2.8	1.96	3.0	1.80	3.1
6	2.18	4.4	2.18	5.0	1.14	3.9	1.19	3.6	1.67	5.5	2.22	3.1	2.01	2.6	1.83	4.1
7	2.12	4.3	2.18	5.9	1.16	3.7	1.16	2.7	1.67	5.6	2.25	2.5	1.95	2.5	1.77	2.9
8	2.11	4.4	2.00	6.7	1.10	3.5	1.12	2.5	1.52	5.9	2.33	3.0	1.93	2.6	1.77	3.2

TABLE XII

^{238}U Absolute Fission-product Rates in Assembly 62

[10^{-17} atoms/(atom ^{238}U)(sec)]

Sample		^{95}Zr		^{97}Zr		^{103}Ru		^{131}I		^{132}Te		^{133}I		^{140}Ba		^{143}Ce	
		Rate	Abs Error, %	Rate	Abs Error, %	Rate	Abs Error, %	Rate	Abs Error, %	Rate	Abs Error, %	Rate	Abs Error, %	Rate	Abs Error, %	Rate	Abs Error, %
Reflector	1	1.44	16.9	1.20	3.5	1.20	5.6	0.411	5.2	1.18	5.8	1.51	5.0	1.26	7.2	0.356	4.4
	2	1.44	13.9	1.45	3.1	1.45	4.8	0.655	9.3	1.39	5.7	1.80	2.9	1.44	5.7	0.525	2.8
	3	1.47	7.0	1.67	3.5	1.67	3.3	0.776	6.3	1.56	5.5	1.83	2.9	1.74	4.6	0.592	9.6
	4	1.88	7.5	2.13	7.9	2.13	3.0	1.03	4.7	1.91	5.6	2.40	3.3	2.02	4.4	0.797	3.2
Interface	1	5.52	5.1	6.25	2.6	6.75	7.4	3.28	2.9	5.59	5.5	7.61	9.0	6.08	2.5	4.09	3.5
	2	5.55	7.2	6.35	2.5	6.97	5.1	3.35	3.1	5.96	5.5	7.74	5.6	6.15	2.7	4.37	2.6
	3	5.82	6.2	6.88	2.6	7.19	3.1	3.88	3.4	6.36	5.6	8.21	3.1	6.84	3.3	4.61	2.6
	4	6.53	3.8	7.51	3.0	8.00	3.7	3.87	3.1	6.90	6.1	9.10	4.9	7.34	2.6	5.27	3.6
	5	7.14	4.5	8.18	2.6	8.53	3.2	4.21	2.9	7.57	5.7	10.2	2.6	7.95	2.8	5.56	3.0
	6	7.40	3.6	8.51	2.6	9.11	2.7	4.54	3.5	8.52	5.5	9.49	2.5	8.65	3.1	6.07	2.7
	7	8.00	5.2	9.00	2.6	9.14	2.6	4.81	2.8	8.02	5.6	9.77	2.5	8.65	3.5	6.11	4.2
	8	7.54	4.1	8.93	2.6	9.42	5.7	4.88	4.1	8.10	5.8	9.55	2.5	8.67	2.7	6.16	3.4
Core	1	12.6	6.6	13.2	6.8	14.6	2.7	7.75	3.6	12.1	6.1	16.1	2.9	13.2	3.8	10.5	4.5
	2	11.4	5.1	12.5	3.0	14.6	2.7	7.60	2.9	11.7	5.8	15.0	2.5	13.1	2.6	10.1	3.8
	3	12.8	4.1	13.1	10.0	14.8	3.3	7.38	2.7	11.6	5.8	15.7	3.4	13.2	2.6	9.98	3.0
	4	11.9	4.9	13.8	3.5	13.9	3.9	7.55	2.7	12.4	5.7	17.0	3.2	13.7	3.8	10.2	3.1
	5	12.5	4.2	14.1	4.2	14.2	2.6	7.70	2.6	12.8	7.8	16.1	3.4	14.1	4.2	9.88	3.4
	6	12.8	3.3	14.5	4.3	14.5	2.9	8.32	3.0	12.9	5.5	16.6	2.5	14.5	2.6	10.5	2.8
	7	13.3	6.7	13.8	3.3	14.0	3.7	7.80	3.4	13.2	5.5	16.8	2.9	14.1	2.6	10.2	2.9
	8	12.4	3.5	13.7	3.0	13.7	3.1	7.75	4.1	12.0	5.9	16.4	4.0	13.3	4.5	9.76	3.2

TABLE XIII. Absolute Fission Rates of ^{235}U and ^{238}U in Assembly 62

Sample Location		Absolute Fission Rate [10^{-15} fissions/atom-sec]			
		^{235}U		^{238}U	
		Rate	Relative Error (%)	Rate	Relative Error (%)
Reflector (0-9)	1	25.5	1.8	0.206	4.2
	2	26.2	1.6	0.241	3.2
	3	26.4	1.8	0.273	2.1
	4	27.0	1.8	0.342	2.5
Interface (0-11)	1	25.5	1.6	1.03	2.1
	2	24.0	1.8	1.06	2.3
	3	24.1	1.9	1.14	1.7
	4	24.2	1.9	1.24	1.6
	5	24.4	2.0	1.34	1.6
	6	25.1	1.5	1.44	1.5
	7	25.4	1.9	1.47	1.6
	8	24.7	1.8	1.46	1.8
Core (0-15)	1	34.8	1.9	2.26	2.2
	2	34.1	1.8	2.18	1.6
	3	34.3	1.9	2.24	2.3
	4	34.0	1.9	2.25	1.8
	5	34.3	1.9	2.32	1.9
	6	35.6	1.8	2.38	1.6
	7	35.2	1.9	2.34	1.9
	8	33.6	2.0	2.24	1.7

TABLE XIV. Spectrum-averaged Cross-section Ratios Measured in Assembly 62

Sample Location		Cross-section Ratio								
		$\frac{^{238}U(n,f)}{^{235}U(n,f)}$	$\frac{^{238}U(n,\gamma)}{^{235}U(n,f)}$	$\frac{^{197}Au(n,\ )^b}{^{235}U(n,f)}$	$\frac{^{58}Ni(n,p)}{^{235}U(n,f)}$	$\frac{^{238}U(n,\gamma)}{^{238}U(n,f)}$	$\frac{^{197}Au(n,\gamma)^b}{^{58}Ni(n,p)}$	$\frac{^{238}U(n,f)}{^{27}Al(n,\alpha)}$	$\frac{^{58}Ni(n,p)}{^{27}Al(n,\alpha)}$
Reflector (0-9)	1	0.0081	0.191	0.863	0.0016	23.6	533	1160	233
	2	0.0092	0.187	0.824	0.0019	20.4	445	1200	241
	3	0.0103	0.186	0.788	0.0022	18.0	352	1120	242
	4	0.0127	0.179	0.737	0.0027	14.1	270	1100	236
	Avg[a]	0.0105	0.186	0.791	0.00217	17.7	364	1150	239
Interface (0-11)	1	0.0404	0.129	0.344	0.0114	3.18	30.2	725	204
	2	0.0442	0.132	0.348	0.0127	2.99	27.4	702	201
	3	0.0473	0.120	0.294	0.0139	2.54	21.1	644	190
	4	0.0512	0.114	0.257	0.0148	2.23	17.4	670	194
	5	0.0549	0.112	0.236	0.0161	2.04	14.6	650	191
	6	0.0574	0.106	0.218	0.0171	1.85	12.7	623	186
	7	0.0579	0.107	0.210	0.0174	1.84	12.1	642	193
	8	0.0591	0.114	0.214	0.0175	1.92	12.2	661	195
	Avg[a]	0.0522	0.116	0.257	0.0153	2.22	16.6	660	194
Core (0-15)	1	0.0649	0.104	0.164	0.0193	1.60	8.52	675	200
	2	0.0639	0.104	0.166	0.0197	1.62	8.41	628	194
	3	0.0653	0.102	0.163	0.0201	1.56	8.13	629	194
	4	0.0662	0.104	0.171	0.0195	1.57	8.77	634	187
	5	0.0676	0.104	0.170	0.0198	1.53	8.60	657	192
	6	0.0669	0.101	0.161	0.0200	1.52	8.05	647	194
	7	0.0665	0.102	0.161	0.0203	1.53	7.92	632	193
	8	0.0667	0.105	0.172	0.0205	1.57	8.37	635	195
	Avg[a]	0.0662	0.103	0.168	0.0199	1.56	8.43	641	193

[a]Drawer-averaged ratios (averaged on the basis of sample weight).

[b]Front gold foil only.

we have converted Maddison's results to reflect the fission rates based upon the ^{97}Zr fission yields measured in the Assembly 60 and 61 tests (5.53% for ^{235}U and 5.44% for ^{238}U). The drawer-averaged fission and reaction rates measured by us (D foil set) and those measured by Maddison (A foil sets) are tabulated in Table XV. Also shown in the table are the results for the gold and nickel foils irradiated on the right side of Half 1 (R foil set) and the ratios of R foils to D foils (R/D).

B. Assembly 63

Table XVI summarizes the absolute fission rates of ^{235}U and ^{238}U at the 15 matrix locations for which measurements were made in Assembly 63. The absolute fission rates were determined by summing the production rates of four individual fission products (^{95}Zr, ^{103}Ru, ^{131}I, and ^{140}Ba) and dividing this sum by the sum of the individual fission-product yields. The relative errors quoted in Table XVI were determined by a propagation-of-error analysis and include all uncertainties with the exception of the errors associated with the fission yields and detector efficiencies.

The fission-rate results are also plotted in Figures 6-9 to illustrate the effects of position and composition upon the measured fission rates. The type of EBR-II subassembly which the various drawers were designed to simulate are also indicated in these figures. Figures 6 and 7 show a horizontal fission-rate distribution for ^{235}U and ^{238}U, respectively. Two rates are plotted at each measurement location; the solid lines represent the samples irradiated above the horizontal centerline of the reactor (top half of Row P) and the dashed lines represent the samples irradiated below the horizontal center line (bottom half of Row P). The differences between the solid and dashed lines reflect experimental precision and/or spectral asymmetry around the horizontal centerline. In all cases, the horizontal distributions of fission rates measured in the corresponding top and bottom half of Row P agree within the 2% experimental uncertainty.

Figures 8 and 9 show the vertical distribution of fission rates along column 15 for ^{235}U and ^{238}U, respectively. In these figures, the solid lines correspond to the number 2 and 4 samples and the dashed lines correspond to the number 1 and 3 samples, i.e., the solid lines provide a vertical distribution along the right half of column 15 and the dashed lines provide a vertical distribution along the left half of column 15. The differences between the solid and dashed lines represent the flux gradient across column 15.

Table XVII summarizes the $^{238}U(n,\gamma)^{239}Np$ reaction rates measured at the 15 matrix positions. Both a relative and absolute error are given for each reaction rate. The relative error refers to uncertainties associated with counting statistics and gamma-ray self-absorption effects, and the absolute error is dominated by uncertainties in the detector efficiency but includes all known sources of error (see Ref. 1 for a complete discussion of errors).

Table XVIII summarizes the spectrum-averaged cross-section ratios determined from the sixty samples at the 15 matrix drawer locations.

TABLE XV. Drawer-averaged Fission and Reaction Rates Determined at the Core, Interface, and Reflector Locations for D, R, and A Packets in Assembly 62

Reaction	Foil Packet	Reaction Rate [10^{-15} atoms/atom-sec] Core	Interface	Reflector
$^{235}U(n,f)$	D	34.3	24.5	26.3
	A[a]	36.5	25.6	27.8
$^{238}U(n,f)$	D	2.27	1.28	0.276
	A[a]	2.38	1.27	0.200
$^{238}U(n,\gamma)$	D	3.54	2.84	4.89
	A[a]	3.79	2.75	6.65
$^{27}Al(n,\alpha)$	D	0.00354	0.00194	0.000239
	A[a]	0.00385	0.00218	0.000314
$^{58}Ni(n,p)$	D	0.682	0.376	0.0572
	R	0.681	0.375	0.0479
	A[a]	0.668	0.369	0.0431
	R/D	0.999	0.997	0.837
$^{197}Au(n,\gamma)$	D	5.75	6.30	20.8
	R	5.77	6.99	30.4
	A[a]	5.73	5.79	20.1
	R/D	1.00	1.11	1.46

[a]Data taken from Ref. 5 and converted to above units.

TABLE XVI. Absolute Fission Rates of ^{235}U and ^{238}U in Assembly 63

Matrix Position	Sample	Absolute Fission Rate [10^{-15} fissions/atom-sec]			
		^{235}U		^{238}U	
		Rate	Relative Error (%)	Rate	Relative Error (%)
P-16	1	46.8	2.1	3.15	2.2
	2	47.0	2.1	3.27	2.1
	3	46.3	2.2	3.22	2.2
	4	46.8	2.1	3.22	2.1
P-15	1	45.2	2.2	2.96	2.1
	2	46.6	2.1	3.07	2.4
	3	44.8	2.2	2.96	2.6
	4	46.2	2.2	3.09	2.2
P-14	1	42.2	2.2	2.67	2.2
	2	43.8	2.2	2.84	2.2
	3	42.2	2.2	2.66	2.1
	4	43.6	2.1	2.73	2.4
P-13	1	37.8	2.1	1.90	2.8
	2	40.4	2.2	2.22	2.4
	3	38.0	2.4	1.88	2.2
	4	40.4	2.1	2.14	2.8
M-15	1	39.4	2.1	2.59	2.4
	2	40.6	2.2	2.74	2.5
	3	41.2	2.2	2.82	2.2
	4	41.8	2.2	2.90	2.2
L-15	1	35.1	2.3	1.96	2.4
	2	35.3	2.2	2.06	2.5
	3	37.7	2.2	2.22	2.2
	4	37.4	2.2	2.29	2.3
N-12	1	31.9	2.3	1.78	2.2
	2	33.0	2.2	1.97	2.2
	3	33.2	2.2	1.85	2.2
	4	34.4	2.2	2.06	2.1
P-12	1	33.8	2.1	1.93	2.2
	2	36.0	2.1	2.06	2.3
	3	33.8	2.3	1.91	2.4
	4	35.4	2.1	1.99	2.1
O-15	1	43.5	2.1	2.54	2.0
	2	43.0	2.3	2.61	2.1
	3	43.6	2.1	2.48	2.2
	4	44.9	2.1	2.60	2.2
Q-11	1	31.4	2.2	1.30	2.2
	2	31.1	2.2	1.60	2.2
	3	30.9	2.1	1.37	2.1
	4	31.3	2.1	1.60	2.3

TABLE XVI. (Continued)

Matrix Position	Sample	Absolute Fission Rate [10^{-15} fissions/atom-sec]			
		^{235}U		^{238}U	
		Rate	Relative Error (%)	Rate	Relative Error (%)
P-11	1	31.4	2.4	1.38	2.5
	2	31.4	2.3	1.66	2.4
	3	31.2	2.2	1.30	2.6
	4	31.0	2.2	1.61	2.0
O-11	1	30.0	2.3	1.57	2.0
	2	31.6	2.4	1.72	2.7
	3	30.6	2.1	1.48	2.4
	4	31.5	2.1	1.76	2.3
P-10	1	34.6	2.2	0.540	2.9
	2	33.7	2.3	0.815	2.4
	3	35.1	2.2	0.548	2.7
	4	33.5	2.2	0.771	2.9
K-15	1	33.8	2.1	1.29	2.7
	2	32.2	2.4	1.50	2.4
	3	33.4	2.3	1.65	2.6
	4	33.2	2.3	1.82	2.0
J-15	1	36.2	2.2	0.516	2.5
	2	35.5	2.1	0.566	3.0
	3	35.1	2.3	0.755	2.5
	4	33.8	2.2	0.845	2.7

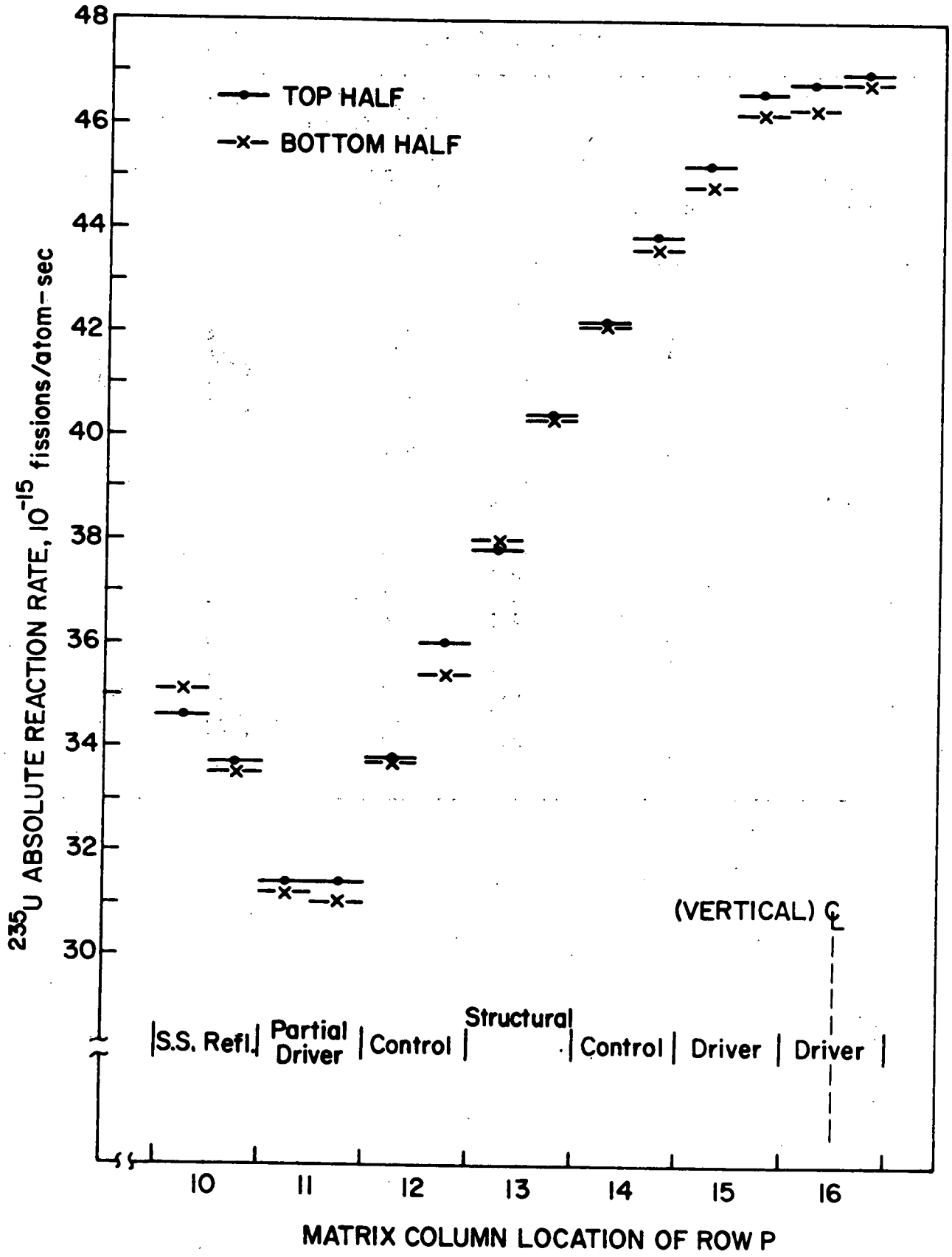

Fig. 6. Horizontal Distribution of ^{235}U Fission Rates in Assembly 63

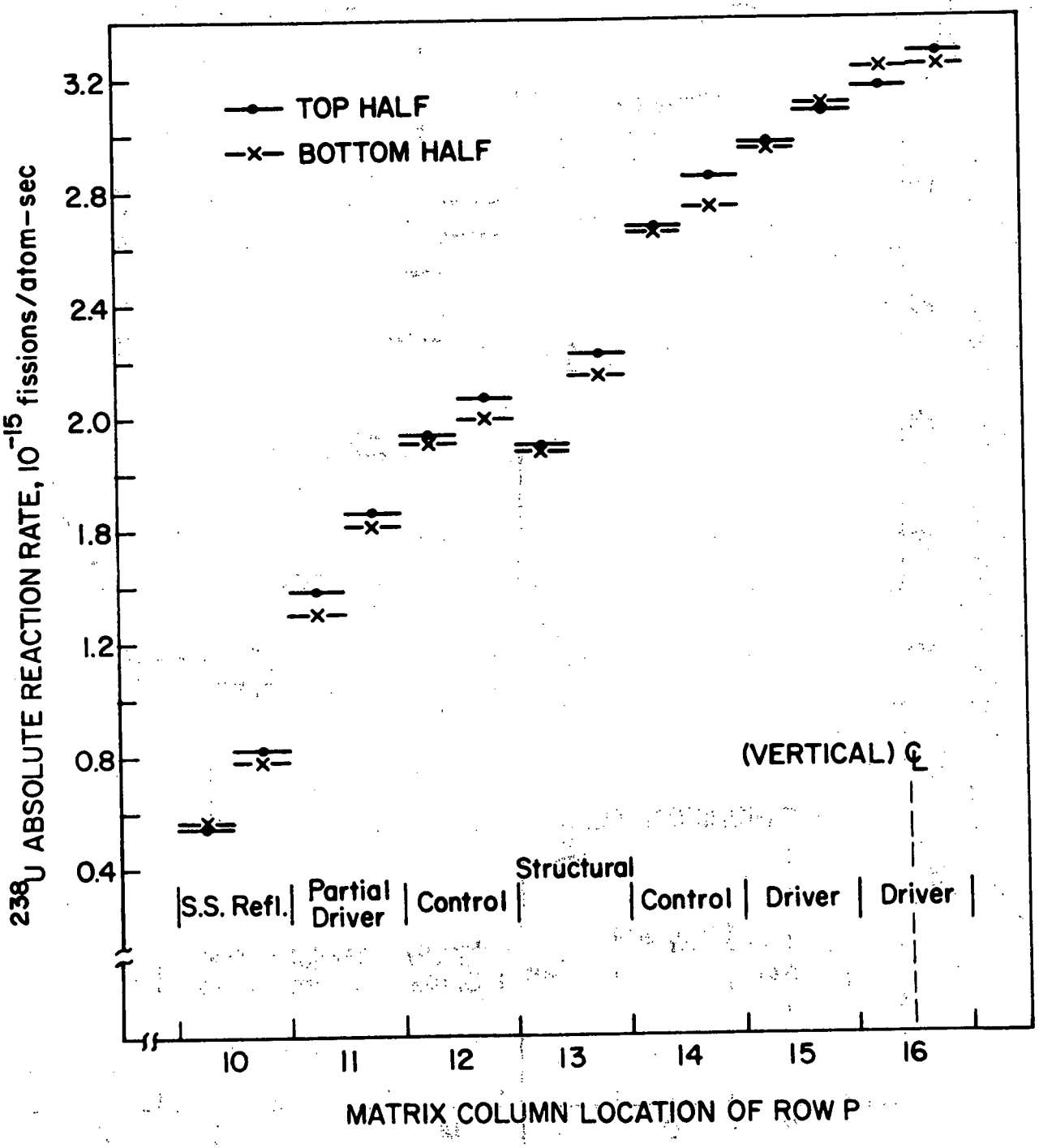

Fig. 7. Horizontal Distribution of ^{238}U Fission Rates in Assembly 63

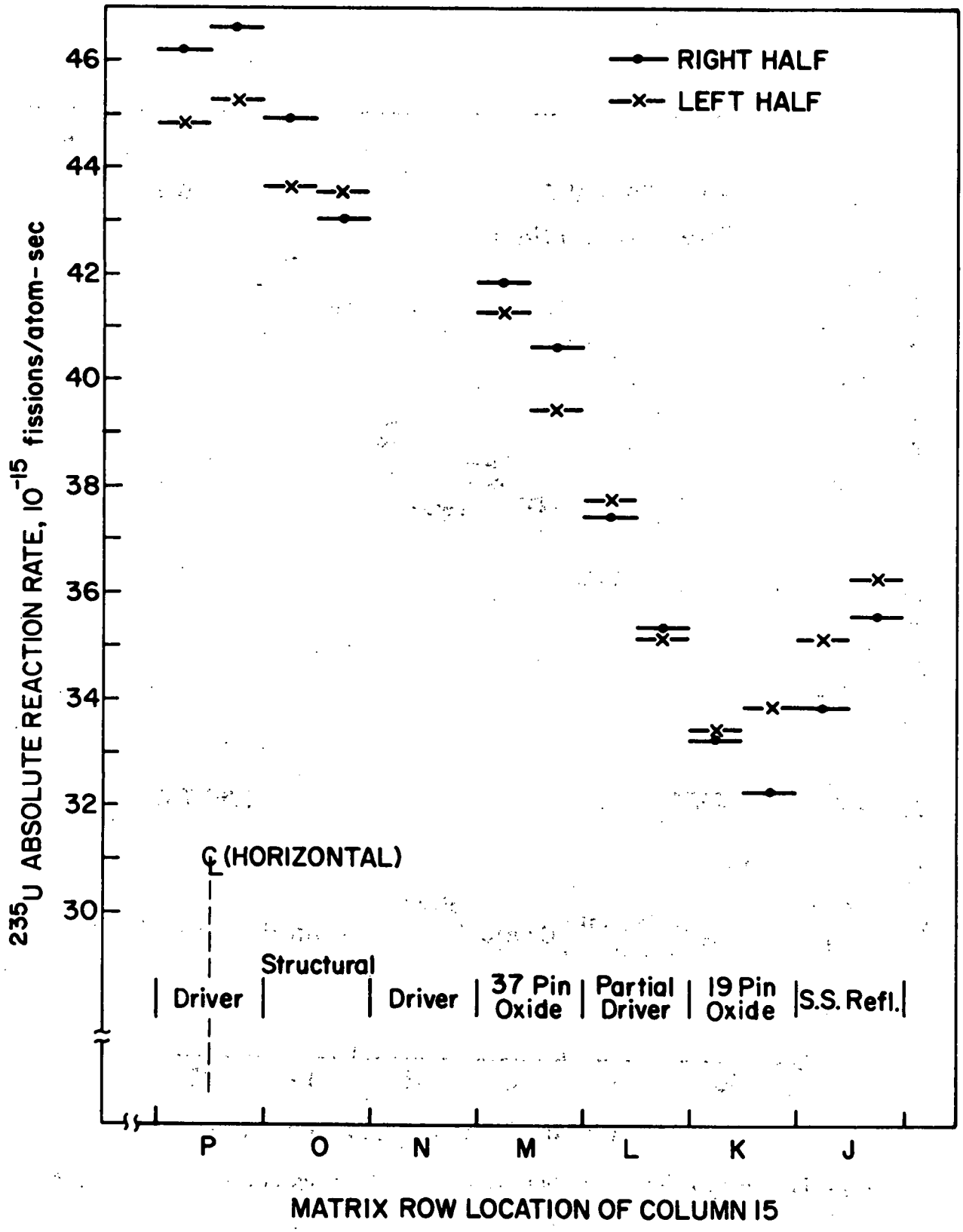

Fig. 8. Vertical Distribution of ^{235}U Fission Rates in Assembly 63

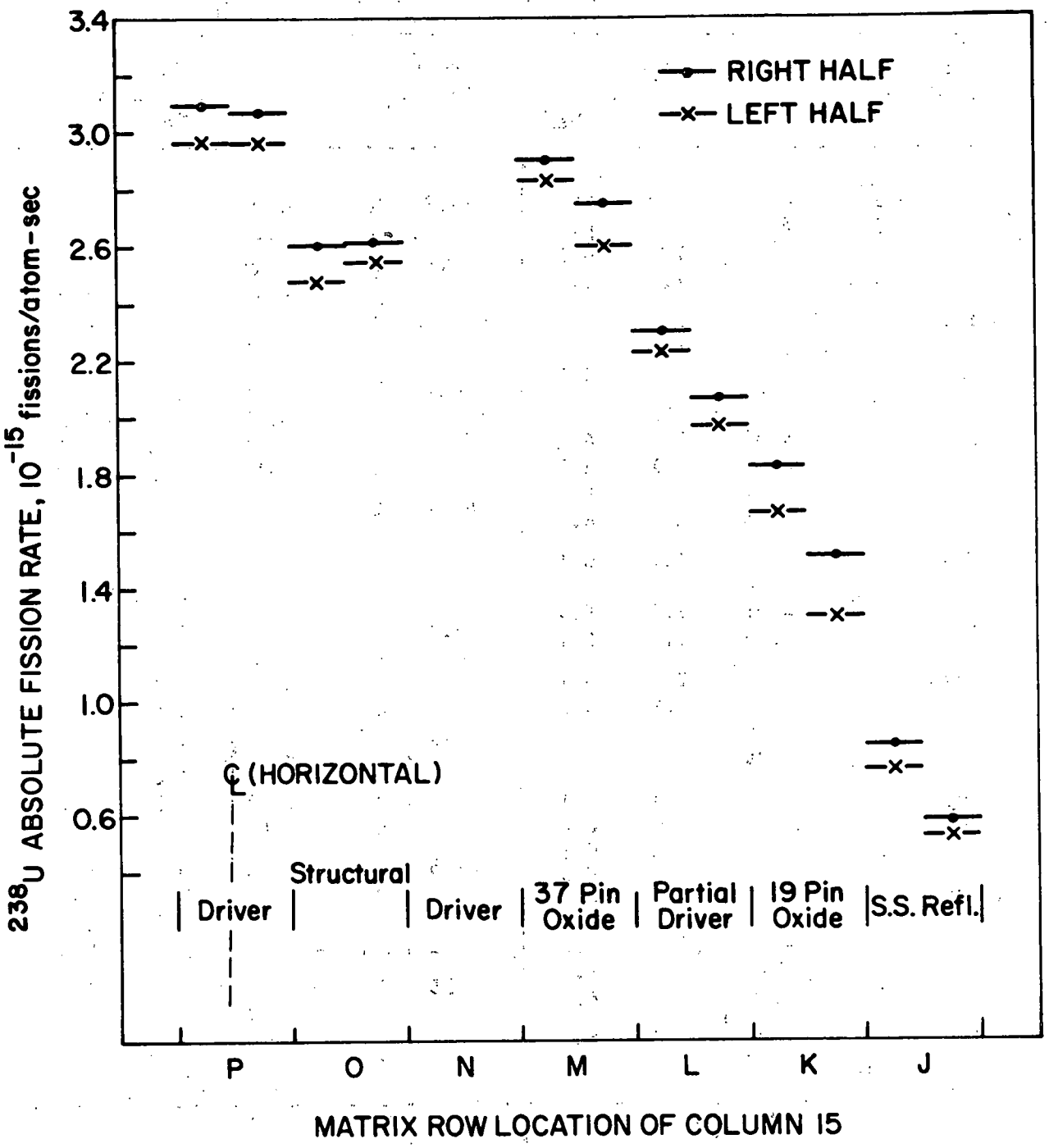

Fig. 9. Vertical Distribution of ^{238}U Fission Rates in Assembly 63

TABLE XVII. Absolute Reaction Rates of $^{238}U(n,\gamma)^{239}Np$ in Assembly 63 [10^{-15} atoms/(atom ^{238}U)(sec)]

Matrix Position		^{239}Np Rate	^{239}Np % Error Rel	^{239}Np % Error Abs	Matrix Position		^{239}Np Rate	^{239}Np % Error Rel	^{239}Np % Error Abs
P-16	1	4.95	1.2	6.1	P-12	3	4.09	1.3	6.2
	2	4.89	1.2	6.1		4	4.22	1.5	6.2
	3	4.90	1.0	6.1	O-15	1	4.81	1.0	6.1
	4	4.88	1.2	6.1		2	5.16	1.5	6.2
P-15	1	4.81	1.0	6.1		3	4.82	0.9	6.1
	2	4.97	1.0	6.1		4	5.27	2.7	6.6
	3	4.80	0.9	6.1	Q-11	1	4.86	1.2	6.1
	4	5.11	1.3	6.2		2	4.29	1.3	6.2
P-14	1	4.58	1.0	6.1		3	4.66	1.2	6.1
	2	4.67	1.1	6.1		4	4.16	1.5	6.2
	3	4.74	2.0	6.3	P-11	1	4.08	1.1	6.1
	4	4.85	2.3	6.4		2	3.77	1.3	6.2
P-13	1	4.53	1.1	6.1		3	4.42	1.3	6.2
	2	4.64	0.9	6.1		4	4.07	1.3	6.2
	3	4.58	2.3	6.4	O-11	1	4.23	1.2	6.1
	4	4.86	1.0	6.1		2	4.16	1.6	6.2
M-15	1	4.41	0.9	6.1		3	4.34	1.4	6.2
	2	4.72	1.9	6.3		4	4.15	0.9	6.1
	3	4.46	1.0	6.1	P-10	1	6.34	1.0	6.1
	4	4.96	2.0	6.3		2	5.44	1.0	6.1
L-15	1	4.05	0.8	6.1		3	7.11	1.1	6.1
	2	4.28	2.0	6.4		4	6.05	1.2	6.1
	3	3.86	1.1	6.1	K-15	1	4.94	0.8	6.1
	4	4.39	2.2	6.4		2	4.75	1.1	6.1
N-12	1	3.97	1.9	6.3		3	4.46	1.0	6.1
	2	4.09	1.5	6.2		4	4.53	1.7	6.3
	3	4.20	1.2	6.1	J-15	1	6.83	1.0	6.1
	4	4.14	1.2	6.1		2	7.07	2.1	6.4
P-12	1	3.86	1.2	6.1		3	6.03	1.4	6.2
	2	4.05	1.3	6.2		4	6.14	1.3	6.2

TABLE XVIII. Spectrum-averaged Cross-section Ratios in Assembly 63

Matrix Position		$\frac{^{238}U(n,f)}{^{235}U(n,f)}$	$\frac{^{238}U(n,\gamma)}{^{235}U(n,f)}$	$\frac{^{238}U(n,\gamma)}{^{238}U(n,f)}$
P-16	1	0.0673	0.106	1.57
	2	0.0696	0.104	1.50
	3	0.0695	0.106	1.52
	4	0.0688	0.104	1.52
P-15	1	0.0655	0.106	1.63
	2	0.0659	0.107	1.62
	3	0.0661	0.107	1.62
	4	0.0669	0.111	1.65
P-14	1	0.0633	0.109	1.72
	2	0.0648	0.107	1.64
	3	0.0630	0.112	1.78
	4	0.0626	0.111	1.78
P-13	1	0.0503	0.120	2.38
	2	0.0550	0.115	2.09
	3	0.0495	0.121	2.44
	4	0.0530	0.120	2.27
M-15	1	0.0657	0.112	1.70
	2	0.0675	0.116	1.72
	3	0.0684	0.108	1.58
	4	0.0694	0.119	1.71
L-15	1	0.0558	0.115	2.07
	2	0.0584	0.121	2.08
	3	0.0589	0.102	1.74
	4	0.0612	0.117	1.92
N-12	1	0.0558	0.124	2.23
	2	0.0597	0.124	2.08
	3	0.0557	0.127	2.27
	4	0.0599	0.120	2.01
P-12	1	0.0571	0.114	2.00
	2	0.0572	0.113	1.97
	3	0.0565	0.121	2.14
	4	0.0562	0.119	2.12
O-15	1	0.0584	0.111	1.89
	2	0.0607	0.120	1.98
	3	0.0569	0.111	1.94
	4	0.0579	0.118	2.03
Q-11	1	0.0414	0.155	3.74
	2	0.0514	0.138	2.68
	3	0.0443	0.151	3.40
	4	0.0511	0.133	2.60

TABLE XVIII. (Continued)

Matrix Position		$\frac{^{238}U(n,f)}{^{235}U(n,f)}$	$\frac{^{238}U(n,\gamma)}{^{235}U(n,f)}$	$\frac{^{238}U(n,\gamma)}{^{238}U(n,f)}$
P-11	1	0.0439	0.130	2.96
	2	0.0529	0.129	2.27
	3	0.0417	0.142	3.40
	4	0.0519	0.131	2.52
O-11	1	0.0523	0.141	2.69
	2	0.0544	0.132	2.42
	3	0.0484	0.142	2.93
	4	0.0559	0.132	2.36
P-10	1	0.0156	0.183	11.7
	2	0.0242	0.161	6.67
	3	0.0156	0.203	13.0
	4	0.0230	0.181	7.85
K-15	1	0.0382	0.146	3.83
	2	0.0466	0.148	3.17
	3	0.0494	0.134	2.70
	4	0.0548	0.136	2.49
J-15	1	0.0143	0.189	13.2
	2	0.0159	0.199	12.5
	3	0.0215	0.172	7.99
	4	0.0250	0.182	7.27

IV. DISCUSSION

A. Left-Right Flux Asymmetry in Assembly 62

The purpose of the D and R foil sets in Assembly 62 was to determine whether flux symmetry existed for physically symmetric reactor locations at which the $^{58}Ni(n,p)$ and $^{197}Au(n,\gamma)$ reaction rates were measured. Table XV presents a comparison of the gold and nickel reaction rates for the left side (D foil set) and right side (R foil set) irradiation positions. The values given in Table XV are averages of the reaction rates determined from the individual pieces of each 2-in. by 2-in. foil. The ratios (R/D) in Table XV are accurate to about 0.2%, since all experimental uncertainties except counting statistics cancel out. These results clearly indicate neutron asymmetry is present in the reflector region.

The reaction rate is a measure of the product $\bar{\sigma}\phi$ where $\bar{\sigma}$ is the spectrum-averaged cross section and ϕ is the flux in units of neutrons per centimeter squared per second. The fact that the reaction-rate ratios R/D are not unity indicates that either $\bar{\sigma}$ or ϕ, or both, are different at physically symmetric interface and reflector locations. Recognizing that the $^{197}Au(n,\gamma)$ reaction is sensitive only to neutrons of energy below $\sim$1 MeV, i.e., to a very soft spectrum such as that which exists in the reflector locations, we must realize that resonances in the eV region may contribute significantly to the observed reaction rate. By comparing the $^{58}Ni(n,p)$ threshold reaction, which is sensitive only to neutrons of energy above $\sim$1 MeV, with the low-energy $^{197}Au(n,\gamma)$ reaction, the following observations can be made from Table XV. Flux and spectral symmetry agree with physical symmetry near the core center of Assembly 62. At the physically symmetric locations near the core-reflector interface, flux symmetry exists for high-energy neutrons, but in the low-neutron-energy region, about 10% more gold activation is observed on the right side of the assembly than on the left. At the physically symmetric reflector locations, neither flux nor spectral symmetry is observed, i.e., the right-side samples experienced a significantly softer and somewhat more intense neutron spectrum than did the left-side samples.

Referring to Fig. 1, we can offer a possible explanation for this effect. The source tube, which consists of a hole through which a neutron source is inserted to initiate criticality, is present on the right side of the reactor. Also, a concrete wall is located within several feet of the right side of ZPR-3, whereas no wall is in close proximity to the left side. Thus, we speculate that neutrons may have leaked out of the source tube and were backscattered off the wall. The leakage would have been greatest for high-energy neutrons, which may account for lesser nickel activation on the right side of the assembly. The backscattered neutrons would also contribute a very low energy flux component, which would have been greatest at the right-side reflector location and would have had an energy gradient which decreased from right to left across Half 1. The resonances in the gold foils would be particularly sensitive to these low-energy back-scattered neutrons. Detailed neutronic calculations will be necessary to establish whether the magnitude of leakage out of the source tube and subsequent backscatter off the concrete wall can account for the magnitude of the observed effect.

In Assemblies 60 and 61, fission-yield foils were located in positions on the right side of the reactor, while similar dosimetry foils were located at symmetric left-side positions. In these experiments, the observed fission rates were lower on the right side than on the left side of the reactor, namely, the ^{235}U fission rate was observed to be about 10% lower and the ^{238}U fission rate about 15% lower at symmetric core locations. Qualitatively, this is consistent with the Assembly 62 observations that a softer spectrum exists on the right side of the reactor than on the left. However, since fission rates were not measured at both right and left reactor positions in Assembly 62, a direct comparison cannot be made.

B. Resonance Neutron-absorption in the Gold Foils

To measure the effect of neutron self-absorption effects in the gold monitor foils, three 0.2-mil gold foils were irradiated together in both the reflector and interface dosimetry packets. These results are summarized in Table IX. The three foils designated front, middle, and back are relative to the face of Half 1 or to the front of the drawer. We observed that in the reflector location (0-9), the reaction rate of the middle foil is depressed by about 10% relative to the reaction rates of the front and back foils, and the reaction rate of the front foil is depressed by about 3% relative to the reaction rate of the back foil. At the interface position, the reaction rate of the middle gold foil is depressed by about 3-6% relative to the front and back foils, and the reaction rate of the front foil by about 1% relative to the back foil. These results are in complete agreement with similar measurements conducted in Assembly 62.

This self-absorption effect is most probably due to resonance self-shielding of the 4.9 and 60 eV resonances in the gold capture cross section. This would indicate that in the reflector position, 5 to 15% of the activation cross section is due to neutrons with these resonance energies. Consequently, any detailed flux and spectral determinations utilizing foil-activation data must include considerations of possible resonance effects. Also, the fact that the back foil always receives greater activation than the front foil indicates that the resonance neutron gradient is increasing in a front-to-back direction relative to the drawer. This effect would be most prominent in the stainless steel reflector as a result of neutron scattering in the steel.

C. Accuracy of Fission-yield Values

The fission yields from which the fission-rate results were derived were based upon the fission yields measured in Assemblies 60 and 61.[1,2] To verify the validity of these yields we can utilize the fission-product data measured in Assembly 62 (see Tables XI and XII). The method used to establish the fission rates has been described previously,[1,2] and was used to average out uncertainties in the fission yield. Briefly, the method was to sum the fission-product rates of each sample and divide this sum by the sum of the fission-product yields. Fission-yield sums are 21.31% for ^{238}U and 18.81% for ^{235}U, respectively. An alternative method would be to divide each fission-product rate by the appropriate fission yield to obtain its fission rate, and average these results to obtain the fission rate for the sample.

For purposes of this discussion, we have determined drawer-averaged fission rates using both of the above methods for the fission products ^{95}Zr, ^{97}Zr, ^{103}Ru, ^{131}I, ^{132}Te, and ^{140}Ba. A comparison of results is presented in Table XIX. The error assigned using the alternative method is the standard deviation of the fission rates of the individual fission products from the mean fission rate and is based upon all six fission products. This comparison shows that there is no substantial difference between the two methods for determining fission rates. The standard deviations in the alternative case indicate that the agreement between fission rates as determined from individual fission products is about ±2% for ^{235}U and about ±3% for ^{238}U.

Table XX summarizes the correlation of fission rates based upon a particular fission product with the average fission rates determined from all the fission products. This tabulation shows eight important points: (1) The ratios tabulated in columns 3 and 5 represent a measure of the precision of the fission yields or the degree of self-consistency among the fission yields. (2) The errors assigned in columns 3 and 5 are standard deviations of the ratios as determined from the various samples given in Tables XI and XII; thus the errors represent the degree of consistency of the ratios for all samples in Assembly 62. (3) The fission yield of ^{131}I for ^{238}U fission is too large by about 15%. (4) The remaining fission yields for ^{238}U fission are, except for ^{95}Zr, very self-consistent; variations of about 6% in the ^{95}Zr results indicate that the largest variation in counting data existed for this nuclide. (5) Use of the ^{140}Ba fission yield for determining fissions of ^{238}U is the most reliable, since its absolute magnitude is quite precise. Only a 1.7% deviation from sample to sample was observed, which indicates good counting data. (6) The fission yield of ^{97}Zr appears to be ∿8% low, and the fission yield of ^{131}I appears to be about 6% high for ^{235}U fission. (7) ^{140}Ba appears to be the best fission-rate monitor for ^{235}U fission, as well as ^{238}U fission. (8) In general, the deviations from sample to sample are much smaller for the ^{235}U fission products (∿2% variations) than for the ^{238}U fission products (∿4% variations).

In summary, we have demonstrated that the two methods for determining fission rates based upon fission-yield information give the same results and that the accuracy of the measured fission rates are dominated by the accuracy of the fission-yield data. The ^{131}I fission yield appears to be low and exhibits the most inconsistency. Similarly, for this type of low fluence irradiation, the ^{95}Zr results exhibit sizable inconsistencies (4-6%). We may conclude, therefore, that fission rates based solely on ^{140}Ba would be more accurate than those obtained by using multiple fission products.

D. Comparison of Fission-rate Traverses By Means of Foils and Fission Counters

In addition to the foil measurements, fission-counter traverses were also carried out in Assembly 63. The results of the ^{238}U and ^{235}U fission-counter traverses in the P row of Assembly 63 are shown in Ref. 5. The foil data enable us to construct similar fission-rate traverses. The comparison of foil data and counter traverses are shown in Fig. 10 for ^{235}U and Fig. 11 for ^{238}U. The foil data are plotted as relative fission rates, with the core center value normalized to unity.

TABLE XIX. A Comparison of Methods for Determining Drawer-averaged Fission Ratios

Method	Nuclide	Core	Interface	Reflector
$\frac{\Sigma F.P.}{\Sigma F.Y.}$ 4 4	^{235}U	34.3	24.5	26.3
	^{238}U	227	128	27.6
$\Sigma_6 \frac{F.P.}{F.Y.}$	^{235}U	34.38±0.62	24.57±0.38	26.01±0.66
	^{238}U	226.3±3.07	125.8±3.12	26.1±1.36
$^{140}Ba \frac{F.P.}{F.Y.}$	^{235}U	34.44	25.00	26.10
	^{238}U	230.6	127.4	27.28

TABLE XX. Fission-yield Correlation

Fission Product	^{238}U F.Y., %	^{238}U F.P./F.Y. Avg. Fiss. Rate	^{235}U F.Y., %	^{235}U F.P./F.Y. Avg. Fiss. Rate
^{95}Zr	5.44	1.029±0.062	6.41	0.998±0.038
^{97}Zr	5.91	1.032±0.015	5.53	1.081±0.020
^{103}Ru	6.29	1.005±0.024	3.29	0.988±0.010
^{131}I	3.66	0.858±0.094	3.44	0.944±0.019
^{132}Te	5.36	1.051±0.031	4.77	0.982±0.023
^{140}Ba	5.92	1.025±0.017	5.67	1.008±0.009

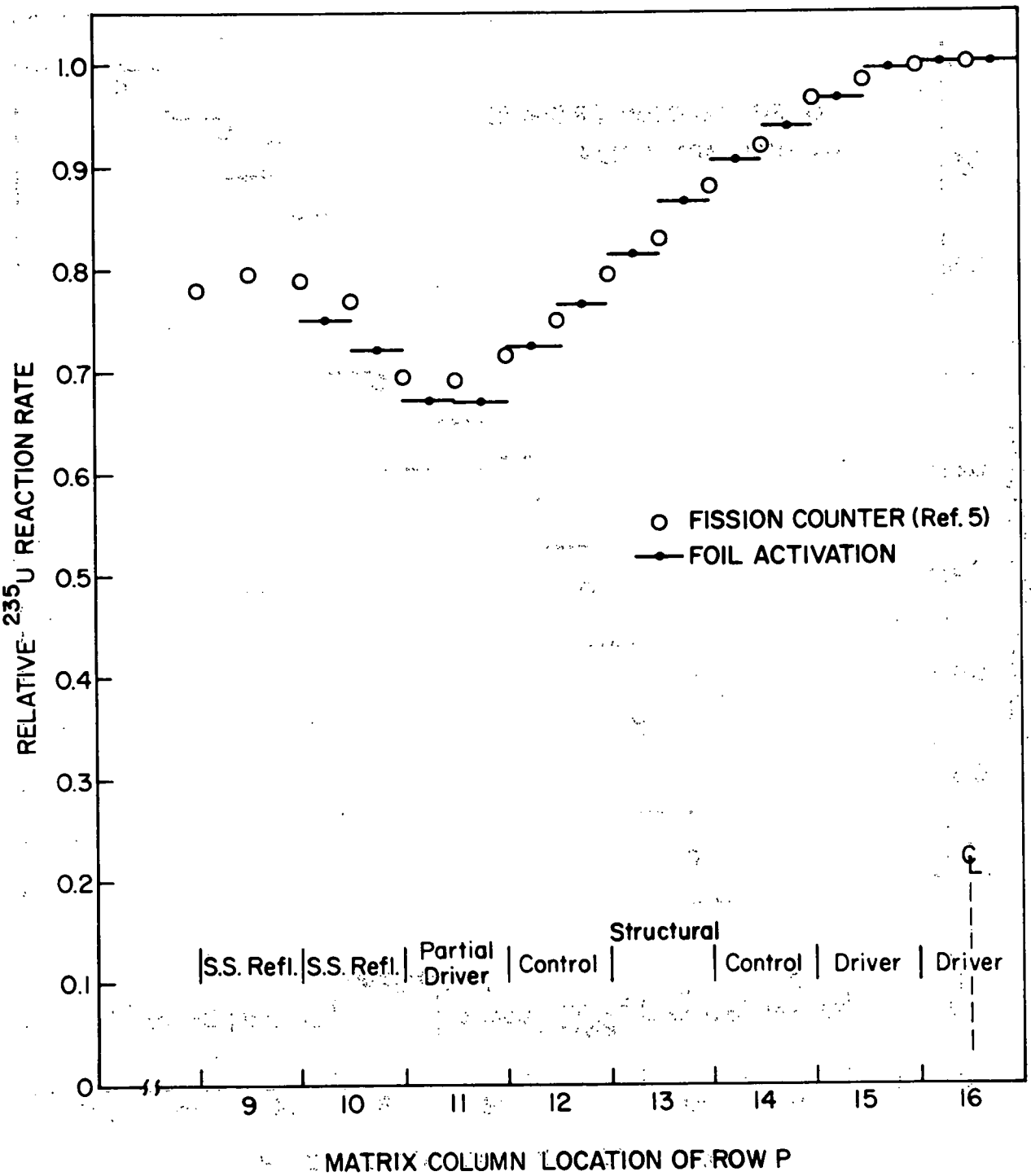

Fig. 10. ^{235}U Foil and Counter Traverses in Assembly 63

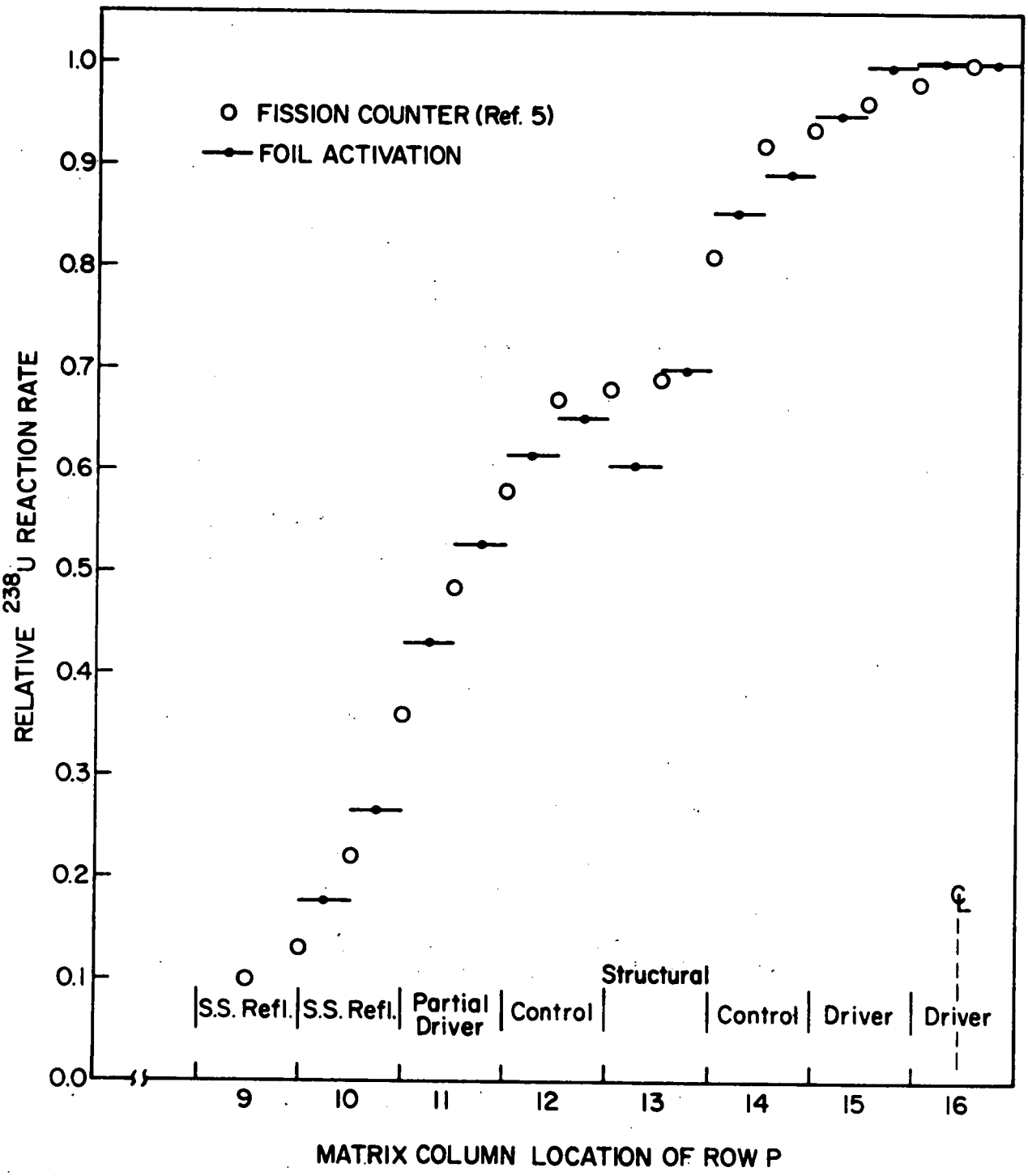

Fig. 11. ^{238}U Foil and Counter Traverses in Assembly 63

Figure 10 indicates very good agreement for ^{235}U fission rates out to drawers 10 and 11, which are a simulated partial driver-type subassembly drawer and a stainless steel reflector drawer, respectively. The foils indicate a more rapid reduction of fission rate in the simulated partial driver subassembly and a less rapid increase in ^{235}U fission rate as one traverses toward the stainless steel reflector. A comparison of foils and counters for ^{238}U fission-rate traverses also shows some minor differences. Most notable is the much greater (~15%) depression indicated by the foils in the simulated structural subassembly in drawer 13. This depression is not nearly so pronounced when measured by the counters. This lessening in depression may be due to the fact that part of the drawer material must be removed to make room for the fission counter, whereas the composition of the drawers is undisturbed by the foil measurements. In addition, the foils provide absolute fission rates, whereas the counters were only utilized in these measurements for relative rates. In general, the agreement between the two techniques is quite good.

E. Neutron Spectral Comparison Between Assembly 62 and 63

Both Assemblies 62 and 63 were designed to simulate EBR-II with a stainless steel radial reflector. However, they differed in one important respect: Assembly 62 was a homogeneous EBR-II core, whereas Assembly 63 simulated various "typical" EBR-II-type subassemblies and for this reason was considered to have a heterogeneous core. In both assemblies, foils were irradiated in the 0-15 (near core center) and 0-11 (near the core-reflector interface) matrix locations. In Assembly 63, the 0-15 position was used to simulate a structural subassembly. In Assembly 62, the composition of all core drawers was identical--a homogeneous representation of the overall composition of EBR-II. The spectrum-averaged cross-section ratios measured in Assemblies 62 and 63 are presented in Tables XIV and XVIII, respectively. In order to make a spectral comparison of the two assemblies, these cross-section ratios are summarized in Table XXI.

TABLE XXI. Spectral Comparison by Cross-section Ratios of Assembly 62 and 63

Location	Assembly	$\frac{^{238}U(n,f)}{^{235}U(n,f)}$	$\frac{^{238}U(n,\gamma)}{^{235}U(n,f)}$	$\frac{^{238}U(n,\gamma)}{^{238}U(n,f)}$
0-15 (Core)	62	0.0662	0.103	1.56
	63	0.0585	0.115	1.96
0-11 (Interface)	62	0.0522	0.116	2.22
	63	0.0528	0.137	2.60

From Table XXI we can make the following generalizations for the specified locations: (1) At the 0-15 position, the spectrum is considerably softer in the structural subassembly of Assembly 63 as compared with that of Assembly 62. (2) At the 0-11 position, the $^{238}U(n,f)/^{235}U(n,f)$ ratios

for Assemblies 62 and 63 are nearly identical, but the $^{238}U(n,\gamma)/^{235}U(n,f)$ ratio and the $^{238}U(n,\gamma)/^{238}U(n,f)$ ratio are larger for Assembly 63 than the corresponding ratios for Assembly 62. This indicates a relative increase in the number of neutrons below about 100 keV in Assembly 63, but the number of neutrons above 100 keV were about the same in each assembly.

The measured reaction rate $\bar{\sigma}\phi$ is the product of the spectrum-averaged cross section times the flux. On the basis of the measured reaction rates, we determine the ratio of ϕ_{63}/ϕ_{62} to be $\sim$1.2. By normalizing the measured reaction rates to the same flux, we can estimate the cross-section ratio $\bar{\sigma}(62)/\bar{\sigma}(63)$ for the three common reactions at the two common irradiation locations. These estimates are:

Location	$^{235}U(n,f)$	$^{238}U(n,f)$	$^{238}U(n,\gamma)$
0-15	1.0	1.13	0.90
0-11	1.0	1.0	0.85

Therefore, at the core position (0-15), we find in Assembly 63 a 13% depression in neutrons of energy >800 keV, and a 10% enhancement of neutrons of energy <100 keV. These effects are due to the structural subassembly configuration of Assembly 63 relative to the homogeneous configuration of Assembly 62. Similarly, at the interface position (0-11), we find an $\sim$15% increase in the number of low-energy neutrons resulting from the 37-pin oxide configuration in Assembly 63 as compared with the number resulting from the homogeneous configuration of Assembly 62.

V. SUMMARY

This report concludes the series describing the activation-rate measurements in the ZPR-3 Mockup Critical Experiments. Perhaps the most valuable results from the mockup experiments have been the determinations of valid fast-neutron fission yields for use in EBR-II. These fission yields were measured in Assemblies 60 and 61, with the results from Assembly 62 serving to verify their applicability to EBR-II-type fast-neutron environments. Only the yields of ^{131}I seem to be questionable, as shown by the analysis in this report. Preliminary results from the EBR-II tests, as well as results from tests we have made in the Coupled Fast Reactivity Measurement Facility (CFRMF) spectrum (a fast-neutron spectrum similar to EBR-II), all indicate that the ^{140}Ba, ^{103}Ru, ^{95}Zr, and ^{132}Te fission yields presented here are both self-consistent and virtually insensitive to neutron energies within the range of neutron spectra examined.

In summary, this report has described the foil-activation-rate measurements conducted in Assemblies 62 and 63 of the ZPR-3 Mockup Critical Experiments. A more thorough discussion of how these data, as well as the data previously reported for Assembly 60 and 61 experiments, can be utilized for characterizing a reactor environment will be the subject of subsequent reports.

In August 1971, foil-activation-rate measurements were conducted throughout the core and core-blanket interface regions of EBR-II during both low (50 kW) and full (62.5 MW) power operations. This test was conducted with a ^{238}U radial blanket in EBR-II and comparisons of the mockup data described in this series with the EBR-II data, as well as comparisons with reactor physics calculations, should contribute significantly toward characterizing the irradiation environment of EBR-II. These comparisons will be the subject of future reports.

ACKNOWLEDGEMENTS

We gratefully acknowledge the discussions and encouragement of D. Meneghetti and W. B. Loewenstein, which enabled us to successfully complete the mockup critical program. W. P. Keeney, J. M. Casidlo, R. O. Vosburgh, and the operating staff of ZPR-3 were particularly valuable in loading, irradiating, and removing the samples from the reactor. H. J. Howard and E. D. Duke of SPM also provided valuable assistance in sample shipments between Illinois and Idaho.

REFERENCES

1. N. D. Dudey, R. R. Heinrich, R. J. Popek, R. P. Larsen, and R. D. Oldham, Activation Rate Measurements in the ZPR-3 Mockup Critical Experiments. Part I. Measurements of Foil-Activation Rates and Fission Yields in Assembly 60 of ZPR-3--Mockup of EBR-II with a Uranium Blanket, ANL-7781 (April 1971).

2. R. R. Heinrich, N. D. Dudey, R. J. Popek, R. P. Larsen, and R. D. Oldham, Activation Rate Measurements in the ZPR-3 Mockup Critical Experiments. Part II. Measurements of Foil Activation Rates in Assembly 61 of ZPR-3 Mockup of EBR-II with a Nickel Reflector, ANL-7926, (March 1972).

3. W. P. Keeney, R. O. Vosburgh, and D. Meneghetti, pp. 34-38 in Reactor Development Program Progress Report, August 1970, ANL-7737 (September 1970).

4. W. P. Keeney, R. O. Vosburgh, and D. Meneghetti, pp. 24-25 in Reactor Development Program Progress Report, November 1970, ANL-7758 (December 1970).

5. D. W. Maddison, ibid, pp. 20-23.

6. W. P. Keeney, R. O. Vosburgh, and D. Meneghetti, ibid, pp. 14-20.